HAARP-Induced Ionospheric Ducts

Gennady Milikh and Aram Vartanyan

University of Maryland, College Park, MD, 20742, USA

Abstract. It is well known that strong electron heating by a powerful HF-facility can lead to the formation of electron and ion density perturbations that stretch along the magnetic field line. Those density perturbations can serve as ducts for ELF waves, both of natural and artificial origin. This paper presents observations of the plasma density perturbations caused by the HF-heating of the ionosphere by the HAARP facility. The low orbit satellite DEMETER was used as a diagnostic tool to measure the electron and ion temperature and density along the satellite orbit overflying close to the magnetic zenith of the HF-heater. Those observations will be then checked against the theoretical model of duct formation due to HF-heating of the ionosphere. The model is based on the modified SAMI2 code, and is validated by comparison with well documented experiments.

Keywords: ionospheric ducts, radio waves, electron heating.
PACS: 94.05.Pt, 94.20.Tt, 94.20.wj, 94.20.Bb

INTRODUCTION

It is well known that the presence of field aligned density striations plays a critical role in the propagation of whistler waves in the ionosphere. These density structures serve as ducts for VLF/ELF wave propagation since the density gradient perpendicular to the magnetic field can lead to their total internal reflection [*Streltsov,* 2007]. Such density structures have often been observed [*Carpenter* et al., 2002] to extend over distances covering entire magnetic field lines. They are known to tap and guide whistler-mode waves between conjugate regions [e.g. *Koons*, 1989]. In fact the presence of such ducts is often considered as a pre-requisite to the generation of Artificially Stimulated Emissions, which have been extensively studied using the Siple VLF transmitter [*Helliwell,* 1988], as well as more recently by the HAARP heater [*Inan et al.,* 2004]. In the HAARP case the VLF waves were generated by modulating the auroral electrojet current at VLF frequencies [see for example *Papadopoulos et al.,* 2003; *Papadopoulos et al*., 2005; *Ferraro et al.,* 1989; and *Barr and Stubbe*, 1993].

Recent experiments detected large scale ducts caused by the HF-heating at HAARP [*Milikh* et al., 2008]. During this experiment the low orbit satellite DEMETER [*Berthelier* et al., 2006a,b] was used as a diagnostic tool which allows one to conduct in situ measurements of the electron and ion temperature and density along its orbit near the magnetic zenith of HAARP. The satellite flies at an altitude of 700 km having an orbit inclination of 98.3^{o}. The experiment shows plasma ducts with the spatial scale of several tens of kilometers. Similar observations were made by DEMETER when overflying the SURA HF-heater [*Frolov* et al., 2008].

The possibility for artificially creating such trans-hemispheric ducts was discussed by *Perrine et al.* [2006]. In that paper it was shown that long term (> 15 minutes) continuous HF-heating of the F-region by powerful ionospheric heaters such as HAARP generates a strong thermal wave in the ionospheric and magnetospheric plasma. This thermal wave propagates along the magnetic field line through the topside ionosphere and magnetosphere, driving ion outflows, displacing the ambient plasma and leading to the formation of density ducts that stretch along the magnetic field line to the conjugate point.

It is the objective of this paper to present observations of the plasma density perturbations caused by the HF-heating of the ionosphere by the HAARP facility. Those observations will be then checked against the numerical model of the artificial ducts.

EXPERIMENTS AT HAARP

A number of experimental tests were conducted at HAARP since 2007. In all of the tests the transmitted power was 3.6 MW, O- mode and the beam was directed along the HAARP magnetic zenith, at which point the modified ionosphere was sensed by DEMETER. Two instruments on-board of DEMETER

were used, the ISL (Lagmuir Probe) that measures the electron density and temperature, and the IAP (Plasma Analyzer Instrument) that measures the ion temperature and composition (O^+, H^+, He^+) [*Berthelier et al.,* 2006a,b].

The DEMETER satellite overflies HAARP twice per day - nighttime and daytime. High density ionospheric ducts were detected predominantly during the nighttime (6-7 UT) observations. Overall we collected about 15 of such observations during 2007-2009 campaigns. Typically the observations reveal a broad peak of electron and O^+ ions densities, often accompanied by peaks of the electron and ion temperature. They were observed along the satellite trajectory, and can reach the length scale of 1000-1500 km while having a fine structure. It is also observed that in many cases increase in O^+ density leads to reduction of H^+ and He^+ density. Thus the lighter ions were pushed upward by the influx of O^+ ions.

We discuss below an illustrative example of the DEMETER observations made on 04/29/08. During this time the on-site diagnostics indicated a weak F-region layer, negligible D/E region absorption and absence of electrojet current. We used a heating frequency of 3.2 MHz. Figures 1 and 2 show key measurements made by DEMETER as it passed 22 km from the center of the heated region. Figure 1 shows ion temperature and density profiles, while Figure 2 shows electron temperature and density. The x-axis shows the time in UTC, longitude and latitude of the satellite location as well as the L-shell it is crossing. The arrows indicate the HAARP location. The peak in the ion temperature and density lasted for about 45 seconds, which corresponds to a distance of 315 km since DEMETER has a velocity of 7 km/s. The electron density peak has a similar duration. The peak in the electron temperature lasted almost a minute, corresponding to 420 km. Earlier *Milikh et al.* [2008] noticed that peaks of the electron and ion density

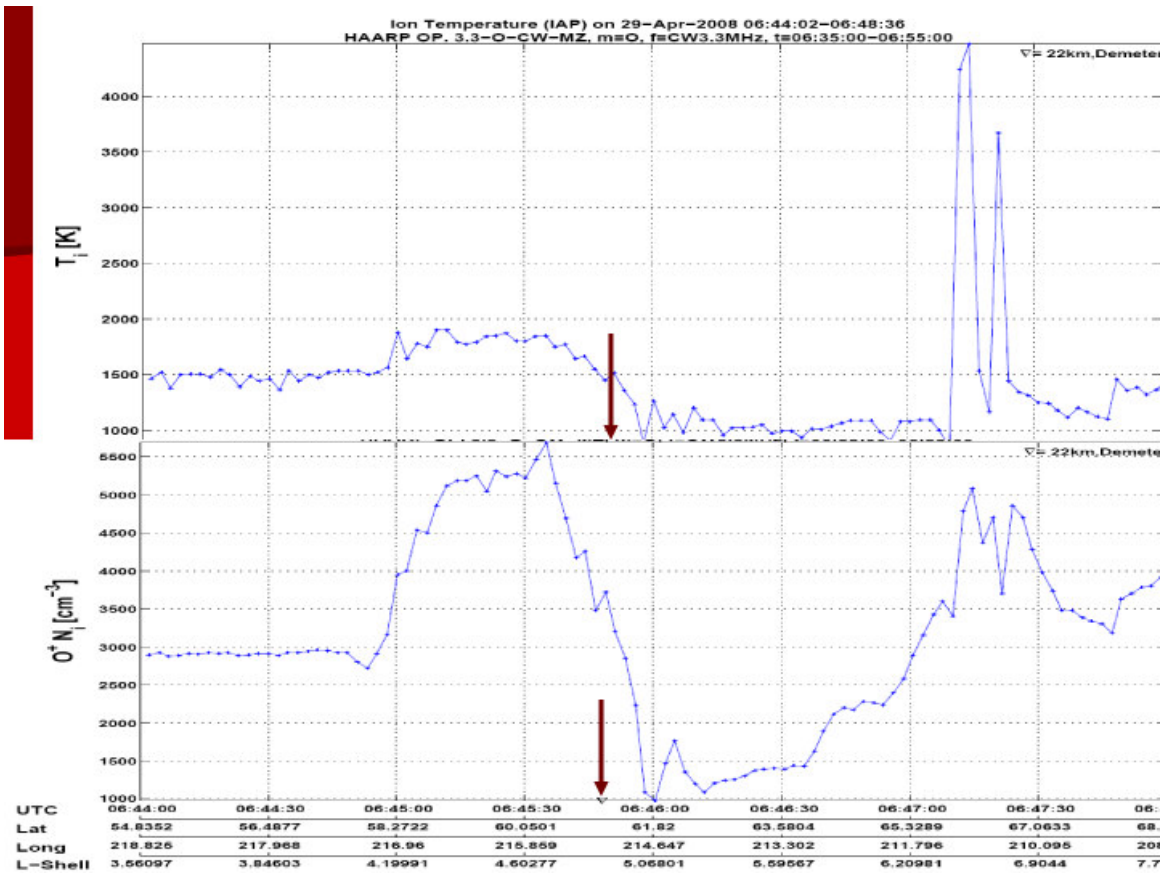

FIGURE 1. The ion temperature and O^+ density measured by Demeter during artificial heating on 04/29/08. The x-axes show the time of the observations, along with the corresponding satellite latitude, longitude and L-shell. The arrows indicate the magnetic zenith of the HAARP location.

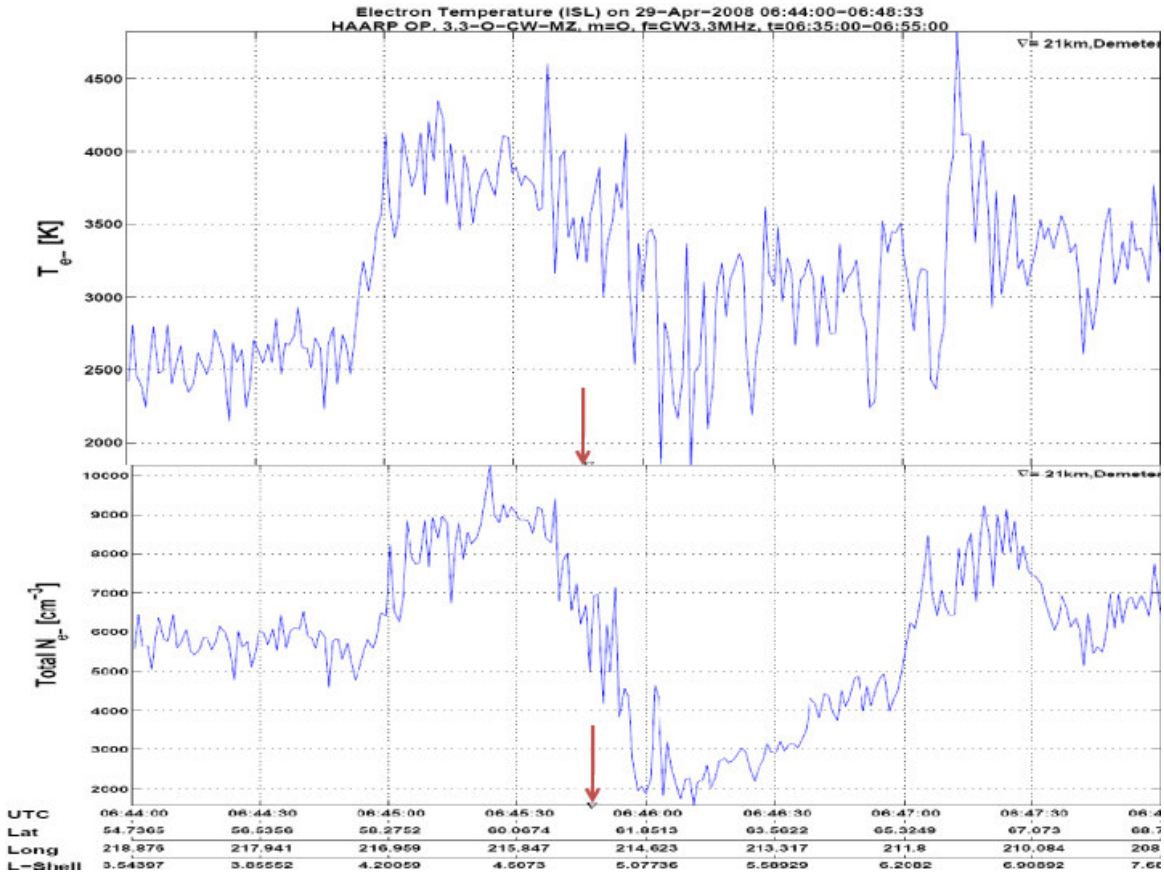

FIGURE 2. The electron temperature and density measured by Demeter during artificial heating on 04/29/08. The x-axes show the time of the observations, along with the corresponding satellite latitude, longitude and L-shell. The arrows indicate the magnetic zenith of the HAARP location.

and temperature can be of different width and can be shifted. It was attributed to the existence of two different transport mechanisms. First, the thermal wave caused by the electron heating transfer excess energy to ions. Later on the heating perturbs the electron density at the heating spot. This creates a temporary pressure imbalance which drives the density perturbations along the magnetic field line leading to ion outflow.

From the observations we obtained the peaks of electron density and electron and ion temperature along with the half width of the O^+ peak. Due to calibration problems values of the peak ion density were miscalculated, although relative variations of the ion density were correct (Michel Parrot, private communications). Since the ionospheric plasma is electro-neutral the ion density is equal to the electron density. The ambient values of the above parameters were taken as average of that at the southward and northward boundaries of the ducts.

All the observations were separated into three groups depending on the ionospheric conditions during the experiments:

(a) The over-dense ionosphere ($f<f_0F_2$).
(b) The under-dense ionosphere ($f>f_0F_2$).
(c) The weak ionosphere when f_0F_2 is not available.

Table 1 shows the average values and error bars of the ambient electron density and its peak value in the ducts found for each of the three groups of observations. It also shows the ambient and peak electron and ion temperatures along with the half width of the ducts. Table 1 reveals that while the ducts in the over-dense and under-dense ionosphere have similar characteristics, in the weak ionosphere the ducts are much narrower. In addition, they have a smaller peak electron density and higher electron temperature. Furthermore, the upward velocity of the ion outflow was estimated based on the following considerations. In the experiments the HF-heating starts 8-10 minutes before the satellite overflies

	$N_e^o\left(cm^{-3}\right)$	$N_e^p\left(cm^{-3}\right)$	$T_e^o(K)$	$T_e^p(K)$	$T_i^o(K)$	$T_i^p(K)$	$L(km)$
Over-dense ionosphere	11600±2150	16500±2450	2960±110	3920±120	1500±80	1800±90	310±210
Under-dense ionosphere	12120±4250	14250±5420	2870±120	3520±220	1500±160	1780±200	430±180
Weak ionosphere	3400±1070	6300±1440	2400±280	4470±510	1180±120	2900±1190	160±50

TABLE 1. The ambient electron density and its peak detected in the ducts (columns 1, 2), the ambient and peak electron temperature (columns 3, 4) and ion temperature (columns 5, 6) along with the half width of the ducts (column 7) found for the over-dense, under-dense and weak ionosphere.

	$F_{duct}\left(\frac{\mu W}{m^2}\right)$	F_{duct}/F_{HAARP}	$P_{duct}(kW)$	P_{duct}/P_{HAARP}
Under-dense ionosphere	0.6	0.01	11.5	3.6×10^{-3}
Over-dense ionosphere	0.32	0.005	8.7	2.7×10^{-3}
Weak ionosphere	0.48	0.0075	4.3	1.3×10^{-3}

TABLE 2. The average energy flux in ducts (column 1), the average ducted energy flux normalized by that generated by HAARP (column 2), the average power pumped into the ducts (column 3), and that normalized by the full power of the HAARP (column 4), all found for the same ionospheric conditions as in Table 1.

HAARP. Since the strong electron heating occurs near the f_0F_2 peak at about 250-300 km, the density perturbations should propagate 400-450 km along the magnetic field line in 8-10 min in order to be detected by the satellite. It gives that the upward velocity V_{up} is of the order of 1 km/s, i.e. on the order of the speed of sound.

Moreover for each of these observations we have estimated the energy flux pumped into the ducts as

$$F_{duct}=[N_e^{peak}(T_e^{peak} + T_i^{peak})-N_e^{0}(T_e^{0} +T_i^{0})]\ V_{up.}$$

Here the first term on the right side of the equation shows the peak energy density inside the ducts while the second term shows the ambient energy density. Estimates of the energy flux are shown in Table 2 averaged for the three groups of experiments conducted at different ionospheric conditions. We have also estimated the total power pumped into the ducts by multiplying the energy flux by the area of the duct $A = \pi\ L_x\ L_y / 4$, where L_x and L_y are the scale lengths along S-N and E-W directions, respectively. While the L_x scale length presents half width of the perturbed region taken from Table 1, the L_y scale length was assumed to be equal to the size of the HF-heated spot. The latter is determined by the HAARP antenna gain which in turn depends upon the radiated frequency.

Finally, Table 2 contains estimates of the ratio of the energy flux and power pumped into the ducts to that irradiated by HAARP. This table reveals that the best conditions for duct production took place in the over-dense ionosphere. In fact, in an over-dense ionosphere maximum power density was pumped into the ducts and thus maximum efficiency of duct production (the last column) was reached.

NUMERICAL MODEL OF DUCT FORMATION

The theoretical/computational modeling employs the SAMI2 code developed at the Naval Research Laboratory [*Huba et al.*, 2000]. The code is an Eulerian grid-based code, which describes an ionosphere made up of seven ion species. The equations of continuity and momentum are solved for the electrons and each ion species, with the temperature equation solved for the electrons and the species H^+, He^+, and O^+. Electron density is determined on the basis of charge neutrality. The code includes *E x B* drift of the field lines with frozen-in

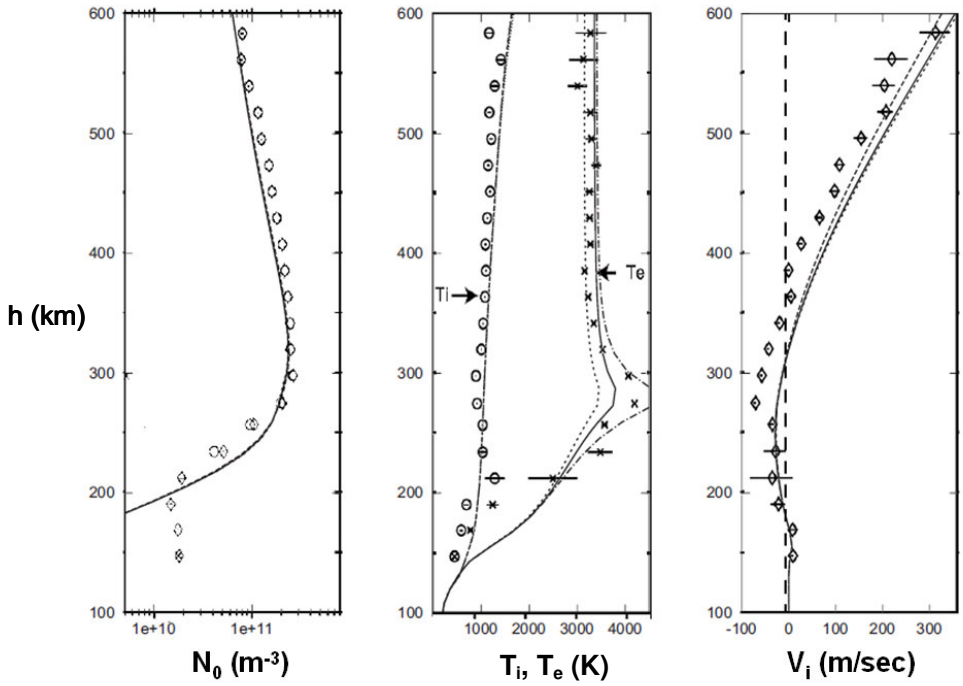

FIGURE 3. The left panel shows the altitude profile of the electron density (circles) observed at EISCAT [*Rietveld et al.* [2003] for the interval started on 10/07/99 at 19:24:00 UT and lasted for 4 min., and that computed by the SAMI2 model (continuous trace). The middle panel shows the observed ion temperature (circles) and electron temperature (crosses) along with the three traces generated by SAMI2 model. Here the points, solid line, and dotes corresponds to the heating rate efficiency μ = 0.16, 0.32 and 0.64 respectively. The far right panel shows the observation of ion velocity (diamonds) along with the three traces which correspond to the computations made at μ = 0.16, 0.32 and 0.64 (from left to right).

plasma (in altitude and longitude), an empirical neutral atmosphere model, horizontal winds, photo-deposition into the ionosphere, ion chemistry models, and ion inertia. This inclusion of ion inertia is critical since it allows for the study of sound wave propagation in the plasma. The SAMI2 model is inter-hemispheric and can simulate the plasma along the entire dipole magnetic field line.

We implement the most recent version of the SAM12 code (release 0.98) which allows us to describe processes at high latitudes. Similar to our earlier paper [*Perrine et al.,* 2006] a flexible local source of the electron HF-heating was introduced in SAMI2 code in the form of localized heating rate per electron. A strong electron heating occurs in an altitude range having the vertical extent between the wave reflection point and the upper hybrid height, which is dominated by the anomalous absorption [*Gurevich et al*., 1996]. Therefore a critical parameter of the model is the absorption efficiency of the incident HF radiation, μ. Notice that the current model does not take into account changes in the F_2 peak electron density induced by the HF-heating, which in turn can affect the absorption efficiency of the heating wave. Such effects will be a subject of our future studies.

The code starts up from empirically determined initial conditions 24 hours before the specific heating time, and runs for 24 hours of 'world clock time'. This practice allows the system to relax to ambient conditions. Also, the neutral density model was adjusted such that the computed f_0F_2 peak matched the observations. Then the "artificial heater" turns on and begins to pump energy into the electrons, using the specified parameters for that run. Artificial heating continues for some time continuously pumping energy into the electrons at the specified altitude, and the perturbations in ion and electron properties are tracked as they travel along the field line. Then the heater switches off, allowing the ionosphere to relax back to ambient conditions. The latter may also varyaccording to the natural factors which determine the ionosphere dynamics.

In order to isolate and measure the perturbations directly, a duplicate set of runs were made, identical to the run described, but with different absorption efficiency. In addition we conduct one run with no

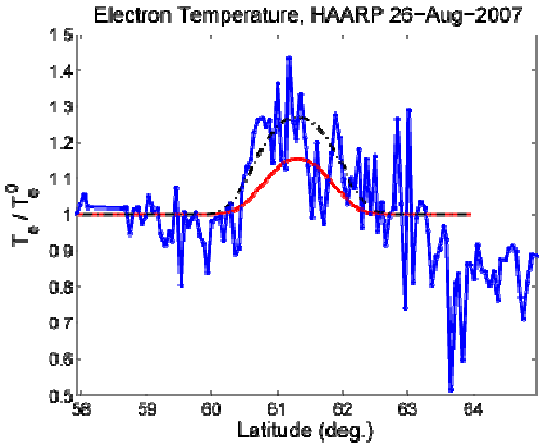

FIGURE 4. Temporary changes in the relative electron temperature computed for the two different absorption efficiencies μ = 0.02 and 0.08 (the bottom and top curves respectively) along with the Demeter observations.

artificial heating which we call an "ambient" or "reference" run, while those with artificial heating are "heated" runs. The ionosphere changes during the simulation due to natural causes, so the perturbations in the heated runs due to artificial heating would not be easily identifiable on their own. But since the same natural variations are present in the ambient data, scaling (or subtracting) by the ambient data provides a simple way to decouple the natural variations from the artificial perturbations.

In this paper the SAMI2 code will be first validated by checking it against the incoherent scatter radar (ISR) observations made at Tromso on 10/07/99 at 19:24 UT [*Rietveld et al.,* 2003]. To model the respective ionospheric conditions we use in the SAMI2 code the A_p and $F_{10.7}$ indexes that were observed at the time of the experiment. The radiated HF power was 960 kW, the half power beam width was 12°, and the facility was operated at a frequency of 4.5 MHz. For those heater and antenna characteristics at EISCAT the heating rate is 12,400 μ, K/s. The absorption efficiency μ is the critical parameter which shows which fraction of the HF energy was absorbed and converted into the electron heating. In our runs the heating rate varied with a range of 2,000 – 8,000 K/s, which corresponds to the absorption efficiency μ = 0.16 – 0.64.

Figure 3 shows the results of our model superimposed onto the observation results presented in Fig. 3 of *Rietveld et al.* [2003]. The latter were made by the European Incoherent Scatter Scientific Association (EISCAT) radar at 19:28 UT. The left panel shows the observed altitude profile of the electron density (circles) and that computed by the SAMI2 model (continuous trace) for 4 minutes in the heating. The middle panel shows the observed ion temperature (circles) and electron temperature (crosses) along with the three traces generated by SAM12 model. Here the points, solid line, and dots corresponds to the absorption efficiency μ = 0.16, 0.32 and 0.64, respectively. Note that the changes in μ affect only the values of electron temperature, while the ion temperature remains unperturbed during a relatively short heating pulse. The rightmost panel shows the observation of ion velocity (diamonds) along with the three traces which correspond to the computations made at different absorption efficiency μ = 0.16, 0.32 and 0.64 (from the left to right). This figure reveals that:

- HF-heating with the efficiency μ =0.3 - 0.6 produces perturbations of the electron temperature which are in good agreement with those detected by the ISR.
- The computed ion velocity fits well with the observations. Namely, it shows that the ion velocity is negative below the heating region, and positive above it. A strong electron heating increases the electron pressure and pushes the plasma both down and upward from the heated region. Thus below this region the ion velocity is negative (downward directed), while above the region it is positive (upward directed) and its value increases with altitude since the plasma propagates in the ionosphere of decreasing density.

Finally we checked our model against the DEMETER observations made above HAARP on 08/26/2007 during an HF heating run. For this purpose we conducted SAMI2 runs for the HAARP location using the specific characteristics of the heater. The heating began 15 minutes before the DEMETER overfly and lasted for about 20 minutes. Figure 4 shows a plot of the electron temperature data as observed by DEMETER 8/26/07 when overflying HAARP, the latter radiated 3.2 MHz radio waves at the maximum power. The DEMETER observations (interpolated points) are superimposed with the SAMI2 code prediction of electron temperature for two different absorption efficiencies μ = 0.02 (short solid hump) and 0.08 (tall dashed hump). The electron temperature is plotted relative to the ambient values. Some explanation of what is meant by ambient is now in order. As mentioned before, computing relative quantities using SAMI2 is accomplished by doing a separate ("reference") run in which the code is run without the introduction of a HF heating term, effectively giving us unperturbed values for the relevant quantities. Since for the DEMETER data this luxury is not present, we took an average of the electron temperature approximately 1 minute prior to the perturbed region and used that average as the

ambient electron temperature. That being said, Figure 4 shows good agreement between the observations and the model for the case of the absorption efficiency μ = 0.08.

In conclusion, observations of ducts caused by the HF-heating at HAARP made by the DEMETER satellite were reported. The best conditions for duct generation occurred in an over-dense ionosphere in the absence of the electrojet. The power pumped into the ducts was estimated as being in the range of 0.1- 0.4% of HAARP's power. It was also shown that the global SAMI2 ionospheric model can be used as a numerical tool to study the artificial ducts.

ACKNOWLEDGMENTS

This work was inspired by Dennis Papadopoulos, with whom we have had many valuable discussions. We also appreciate collaborations with Joe Huba, Glenn Joyce, Andrei Demekhov, Evgeny Mishin, Hira Shroff and Michel Parrot. The work was supported by the ONR Grant NAVY.N0017302C60 and by the ONR MURI Grant N000140710789. The experimental work was supported by the HAARP Program, Air Force Research Laboratory at Hanscom Air Force Base, Massachusetts, through the ONR contract N00014-02-C0463. We acknowledge CNES for the use of the DEMETER data. We acknowledge Mike McCarrick's expert help in conducting the HAARP experiments.

REFERENCES

1. R. Barr and P. Stubbe, *Geophys. Res. Lett.* **20**, 2243-2246 (1993).
2. J. J. Berthelier, M. Godefroy, F. Leblanc, et al., *Planetary Space Sci.* **54**, 456-465 (2006a).
3. J. J. Berthelier, M. Godefroy, F. Leblanc, et al., *Planetary Space Sci.* **54**, 487-497 (2006b).
4. D. Carpenter, D. et al., *J. Geophys. Res.* **107** (A9), 1258, 10.1029/2001JA009199, (2002).
5. A. J. Ferraro, H. S. Lee, T. W. Collins, et al., *IEEE Trans. Antennas Propag.* **37**, 802-809 (1989).
6. V. L. Frolov, V.O. Rapoport, G.P. Komrakov, et al., *Radiophy.s Quantum Electronics* **51**, No. 11 (2008).
7. A. V. Gurevich, A. V. Lukyanov, and K. P. Zybin, *Phys. Lett. A* **211**, 363-372 (1996).
8. R. A. Helliwell, *Rev. Geophys.* **26**, 551-562 (1988).
9. J. D. Huba, G. Joyce and J.A. Fedder, *J. Geophys. Res*. **105**(A10), 23035-23053 (2000).
10. U. S. Inan, M. Golkowsky, D. L. Carpenter, et al., *Geophys. Res. Lett.* **31**, L24805, doi: 10.1029/2004GL021647 (2004).
11. H. C. Koons, *J. Geophys. Res*. **94**(A11), 15393-15397 (1989).
12. G. M. Milikh, K. Papadopoulos, H. Shroff, C.L. Chang, et al. *Geophys. Res. Lett.* **35**, L17104, doi:10.1029/2008GL034630 (2008).
13. K. Papadopoulos, T. Wallace, M. McCarrick, et al., *Plasma Phys. Reports* **29**, 561-565 (2003).
14. K. Papadopoulos, T. Wallace, G.M. Milikh, W. Peter, and M. McCarrick, *Geophys. Res. Lett.* **32**, L13101, doi:10.1029/2005GL023185 (2005).
15. R. P. Perrine, G. M. Milikh, K. Papadopoulos, J. D. Huba, G. Joyce, M. Swisdak, and Y. Dimant, *Radio Sci.* **41**, RS4002, doi:10.1029/2005RS003371 (2006).
16. M. T. Rietveld, M. J. Kosch, N. F. Blagoveshchenskaya, et al., *J. Geophys. Res.* **108**, doi:10.1029/2002JA009543 (2003).
17. A. V. Streltsov, *J. Geophys. Res*. **112**, A12218, doi:10.1029/2007JA012710 (2007).